PVA POLYMER (CAO/CDO/AL$_2$O$_3$) NANOCOMPOSITES: TOWARD IMPROVED SUPER CAPACITOR AND OPTO-ELECTRICAL PROPERTIES

Gayitri H M[1*], Murad Q. A. Al-Gunaid[2], Suma G. R[3], Vidhya C[4], Manimozhi R[5], Kumar J R[6]

Astract

Nanocomposite (NC) films of poly vinyl alcohol (PVA) incorporated with varying amounts of Calcium Cadmium doped Aluminum oxide ($CaCdAl_2O_5$) nanoparticles (NPs) have been fabricated by solution intercalation technique. TEM result showed the size of NPs between 8-34nm. The effects of NPs content on structural and morphological behaviors of PVA have been established by XRD, FTIR and SEM techniques. Electrical properties of NC films were performed by using LCR-meter. Current (I)-voltage (V) graph displayed that dc-conductivity increased with increasing NPs content and trends of I–V indicate the dominant Ohmic behavior at voltage <5V and above that Poole–Frenkel emission is the dominant conduction mechanism. Ac-conductivity increases with increase in frequency and dosage of NPs. The maximum ac-conductivity obtained in this investigation is $2.43x10^{-5}$ S/cm for PVA/8wt% $CaCdAl_2O_5$. The reduction in glass transition temperature T_g with increment in NPs contents was observed. The optical behaviors of NCs were deduced by UV visible spectroscopy where the result showed that band gap energy was reduced from 5.23eV to 3.25eV whereas refractive index increased from 1.71 to 2.44 for pure PVA and PVA/8wt% $CaCdAl_2O_5$ respectively. The calculated C_{spec} values show a significant enhancement in C_{spec} from 1.75F/g for pure PVA to 3.75F/g for PVA/ 8wt% $CaCdAl_2O_5$ NCs.

Keywords: Nanocomposites; band gap energy; refractive index; DC conductivity; glass transition temperature.

[1]*Department of Electronics and Communication Engineering, JSS Science and Technology University, Sri Jayachamarajendra College of Engineering, Mysore 570006, India, email: gayitrikumar@sjce.ac.in , Contact no: 8073378979

[2]Department of Chemistry, Faculty of Education, Thamar University, Dhamar 13020, Yemen

[3]Department of Chemical Engineering, Siddaganga Institute of Technolgy, Tumakuru 572103

[4]Department of Chemical Engineering, RV college of Engineering, Bangalore-560059, Karnataka, India

[5]Department of Physics, Regional Institute of Education, Mysore 570006,

[6]Department of Bio Chemistry, Faculty of Life Sciences, JSS Academy of Higher Education and Research, Mysure-570015

***Corresponding Author:** Gayitri H M

*Department of Electronics and Communication Engineering, JSS Science and Technology University, Sri Jayachamarajendra College of Engineering, Mysore 570006, India, email: gayitrikumar@sjce.ac.in , Contact no: 8073378979

DOI: 10.48047/ecb/2023.12.si10.0079

1. Introduction

The incorporation of hybrid metal oxide nanoparticles (NPs) into transparent polymer matrix-based nanocomposites (NCs) holds significant significance owing to their wide range of potential applications in areas such as polarizers, light-stable color filters, solar cells, and optical sensors [1, 2]. owing to their small size and high aspect ratios, hybrid metal oxide NPs have unique features. The synthesis of metal oxide nanoparticles (NPs) has provided enhanced capabilities in terms of controlling their shape, size, crystallinity, and functionalization, all achieved at a relatively low cost. In order to further support their properties, the metal oxide NPs have been hybridized by multi elements such as $LaAlO_3$, $SrZrO_3$, etc. [3,4]. The perovskite calcium cadmium and aluminate nanoparticles ($CaCdAl_2O_5$) have drawn the most interest among the hybrid metal oxide NPs due to their various uses in catalysis, ferroelectrics, and photoelectrics, particularly their superconductivity property at a lower temperature [5–7]. The incorporation of specific hybrid nanoparticles (NPs) into vinyl polymers based on dielectric materials has been discovered to bring about significant modifications in various characteristics of composite materials. This, in turn, enables their utilization in a wide range of applications such as sensors, electrochromic displays, fuel cell electrodes, electrical igniters, antistatic shielding for electronic components, and even as crucibles for vacuum induction furnaces. [8-10]. Extensive literature research indicates that there exists substantial potential for further enhancing the performance of Polyvinyl Alcohol (PVA) through the utilization of hybridized nanosized fillers. [11–15]. The incorporation of nanoparticles (NPs) into a blended polymer matrix has the potential to enhance the interaction at the interfaces between the polymer and the filler, leading to improved performance. [16]. Currently polymeric nanocomposites with good optical clarity and high refractive index have drawn a great deal of scientific interest because of their potential applications in optical filters, waveguides, lenses, light emitting diodes (LEDs) and reflectors.[17,18]. The most important challenges is the enhancement in the properties of pristine polymers to achieve good conductivity, reduction in optical bandwidth and high optical clarity at lower dosage of NPs. Nevertheless, the optical applications of conventional polymers are constrained by their limited range of refractive indices. (RIs).[19]. There are numerous reports in literature, which shows an increase in conductivity of PVA after incorporation of NPs.[20,21]. Moreover, there is inadequate data in the literature regarding the conduction mechanism of PVA/ $CaCdAl_2O_5$ NCs. Therefore, the main objective in the current investigation is to achieve a deeper consideration of impact $CaCdAl_2O_5$ NPs to tune the band gap, refractive index for PVA matrix and to enhance the electrical conductivity, dielectric permittivity and electrochemical behavior of PVA NC films for optoelectronic applications.

2. Experimental details

2.1. Materials

PVA (average molecular weight 125,000 Aldrich), calcium nitrate (Ca $(NO_3)_2$) (AR grade, SD. Fine chem.,), cadmium nitrate ($Cd(NO_3)_2$), and aluminium nitrate ($Al(NO_3)_3$) (as oxidant) and glycine ($C_2H_5NO_2$) as fuel were purchased from SD Fine-chem. Limited, Mumbai, India. Double distilled water was used in this study.

2.2. Synthesis of cadmium calcium doped aluminum oxide ($CaCdAl_2O_5$) (NPs)

In the current investigation cadmium calcium doped aluminum ($CaCdAl_2O_5$) NPs was synthesized using solution combustion method.[22] The appropriate amounts of calcium nitrate (Ca $(NO_3)_2$), cadmium nitrate ($Cd(NO_3)_2$), and aluminium nitrate ($Al(NO_3)_3$) (where molar ratio of Ca:Cd: Al is (60:40:40) and glycine ($C_2H_5NO_2$) were dissolved in double distilled water, separately. The molar ratio of fuel to oxidant nitrates was 4:1. The individual solutions were then mixed together and the pH value was adjusted to 8.5 by adding NaOH solution. Then the solution was constantly stirred at 90°C for 2 hrs to obtain dark gel. The gel was continuously heated until the combustion process occurred and a loose powder formed. Finally, obtained the cream color powder and was calcinated at 800°C for 4 hrs.

2.3. Casting of PVA/ $CaCdAl_2O_5$ nanocomposite films

PVA of 21g obtained in the powder form was dissolved in 300 ml of doubly distilled water at 80°C for about 2 hrs. Then varying amounts viz., 2, 4, 6 and 8wt % of NPs were added to aqueous PVA solution by mechanical stirring followed by ultrasonication for 30min. The homogeneous solution was poured into a cleaned and releasing agent smeared glass petridish and the solvent was allowed to evaporate slowly at 25° C for 72 hrs to get dry film. Finally, the samples were vacuum dried in a hot air oven at 60°C for 3-4 hrs. The

thickness of the obtained NC films varied from 0.22 to 0.24 mm.

2.4. Characterization

The size and compositional characteristics of synthesized $CaCdAl_2O_5$ NPs are studied by High Resolution Transition Electron Microscope (HRTEM) with JEOL/ JEM 2100, Japan. The structure of pristine $CaCdAl_2O_5$ NPs and doped PVA NCs were obtained at room temperature by X-ray diffraction (XRD) patterns on a D8 Advance-Bruckers AXS diffractometer with Cu-Kα radiation source (λ = 1.54 °A) operated at 40 kV and 40 mA in the 2θ range 10-80° at the scan speed of 0.05° per second. The morphological behaviors of NPs and all NC films were recorded by scanning electron microscope (SEM), Zeiss-108A, Germany. The physical interaction between components was studied by Fourier transform infrared (FTIR) spectra, JASCO 4100

Spectrometer, Japan. All films scanned over the wave number range 4000-500 cm^{-1}. The I-V and ac electrical parameters of films were measured by LCR meter Wayane Kerr-6430, UK at room temperature. The ac-electrical studies have been carried out in the frequency range 50Hz-5MHz at 1V. The surface of films were coated with silver paste and sandwiched between two stainless steel electrodes which having an area of 0.5 cm2. The values of capacitance (C), resistance (R), conductance (Gs) and dissipation factor (tan δ) of the NC films at each excitation frequency were recorded. Electrochemical cyclic voltametry (CV) was performed using CH-Instrument, model 600D series, with potassium hydroxide (2M) as background electrolyte at potential scan rate of 0.1 Vs^{-1}, using Ag/AgCl reference and platinum wire as counter electrodes. The thermal behaviors of the NCs have been evaluated using differential scanning calorimetry (DSC), TA Q200, USA. The weight of sample around 6 mg was scanned at a heating rate of 10°C/min in the temperature range 40–240°C under nitrogen gas purge. The UV–visible spectroscopic studies have been established by Schimadzu-1800 spectrophoto-meter, Japan in the wave length range 200–800 nm.

3. Results and discussion

3.1. Structural and morphological characteristics

The XRD patterns of $CaCdAl_2O_5$ nanofiller and PVA/$CaCdAl_2O_5$ NCs are presented in Figure 1(a) and (b).The XRD pattern showed a crystalline peak at 19.8° refer to main crystalline potions of PVA structure [23]. The pure $CaCdAl_2O_5$ NPs exhibits a distinctive sharp and intense peak at 2θ ~32.9° in addition to multiple strong peaks at 2θ = 38.19, 55, 21, 65, 76, and 69.21° which denote to the obtained $CaCdAl_2O_5$ NPs are well crystallized. The small peaks at 38.19, 55, 21, 65, 76, and 69.21° of PVA/$CaCdAl_2O_5$ NCs denotes to small islands of crystalline portion dispersion in amorphous region in PVA structure [24]. In addition, the main characteristic diffraction peaks of PVA at 2θ =19.8° were slightly shifted to 18.8° with broadening and decreasing in intensity for the NCs films. Such trends may be attributed to the distortions or defects in $CaCdAl_2O_5$ lattice and physical changes in PVA structure due to the interaction between them, which may leads to amorphous effect on the crystalline structure of PVA. The Scherer length (L) that is size of the crystallites for NCs was calculated using X-ray data at wavelength (λ) (CuKα = 0.15406 nm) and Bragg diffraction angle (θ) by using the following equation;

$$L=\frac{0.9\lambda}{\beta\cos\left(\frac{2\theta max}{2}\right)} \qquad (1)$$

where, β is the full width at half maximum of the peak (FWHM). The Scherrer length (L), lattice strain (β cos θ/4) and dislocation density (η = 1/L2) have been calculated for all PVA/ $CaCdAl_2O_5$ films related to the peak at 2θ = 19.8º where, the estimated data are summarized in Table 1. From obtained results, the Scherrer length of doped PVA decreased and FWHM values increases with increase in $CaCdAl_2O_5$ content. That means the peak width (FWHM) inversely proportional to crystallite size, as the crystallite size gets smaller, the diffraction peak broaden. Smaller the values of Scherrer length indicate the amorphous nature of the NC films. It also reveals that the lattice strain and dislocation density values increases with increase in $CaCdAl_2O_5$ contents in NC films, means the defects density affect on the molecular packing of PVA chains. The effect of $CaCdAl_2O_5$ NPs on PVA can be further evaluated by the values of stacking fault (SF) and inter-crystallite separation(R) of NCs from position of maximum haloes,[25] related to diffraction peaks at 2θ = 19.8°, using the relation;

$$SF=\left(\frac{2\pi^2}{45(tan\theta)^{1/2}}\right)\beta, \qquad (2)$$

$$\text{and } R=\frac{5\lambda}{8\,sin\theta} \qquad (3)$$

The obtained values of SF and R for NCs were listed in Table 1. An increment of stacking fault (SF) and inter crystallite separation (R) with

increasing dosage of NPs in NCs was noticed which confirms effect of $CaCdAl_2O_5$ NPs on PVA crystallinity. The trend of R values is consistent with that the values of doped PVA with the data published elsewhere.[25-26]

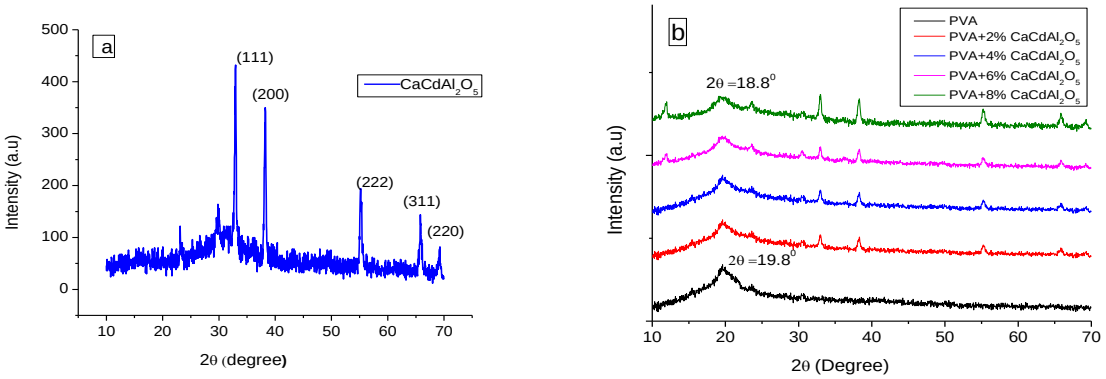

Figure 1(a) The XRD pattern of $CaCdAl_2O_5$ nanofiller and (b) XRD pattern pure PVA and PVA/$CaCdAl_2O_5$ NCs

Table 1: The structural parameters of PVA/ $CaCdAl_2O_5$ NCs at $2\theta_{max}$=19.8º for PVA

No	Composites	$2\theta_{max}$ (Deg)	FWHM, x 10^{-2} (Rad)	d-spacing x 10^{-2} (Å)	Scherer length (L) (Å)	Lattice Strain x 10^{-2}	R	SF
1	$CaCdAl_2O_5$*	32.9	1.39	-	6.51	-		-
2	PVA	19.8	6.78	259	6.95	6.85	326	0.54
3	PVA+ 2%$CaCdAl_2O_5$	19.71	8.54	262	5.78	8.45	327	0.57
5	PVA+ 4%$CaCdAl_2O_5$	19.63	9.61	264	5.60	8.66	330	0.63
6	PVA+ 6%$CaCdAl_2O_5$	18.92	9.74	265	5.57	9.79	333	0.70
7	PVA+ 8%$CaCdAl_2O_5$	18.83	9.85	267	5.18	9.87	335	0.74

$CaCdAl_2O_5$* the parameters of pure NPs calculated respected to $2\theta_{max}$=32.9º. All calculated values depend on θ in radians

The Transition electron microscope (TEM) was carried out to determine size for pristine $CaCdAl_2O_5$ NPs obtained by calcinating at 750°C (Figure 2(a)). The TEM image reveals that NPs shape is uniformly distributed with nanoporous where the particle size lies in the range 8-55 nm and accord with outcomes for same NPs mentioned elsewhere [27]. The pore generation during gaseous product evolution was further confirmed from the TEM image. The bright spots on the SAED pattern of NPs indicate the crystal structure of obtained $CaCdAl_2O_5$ NPs, which is in consistent with the XRD interpretation as shown in figure 2(b)

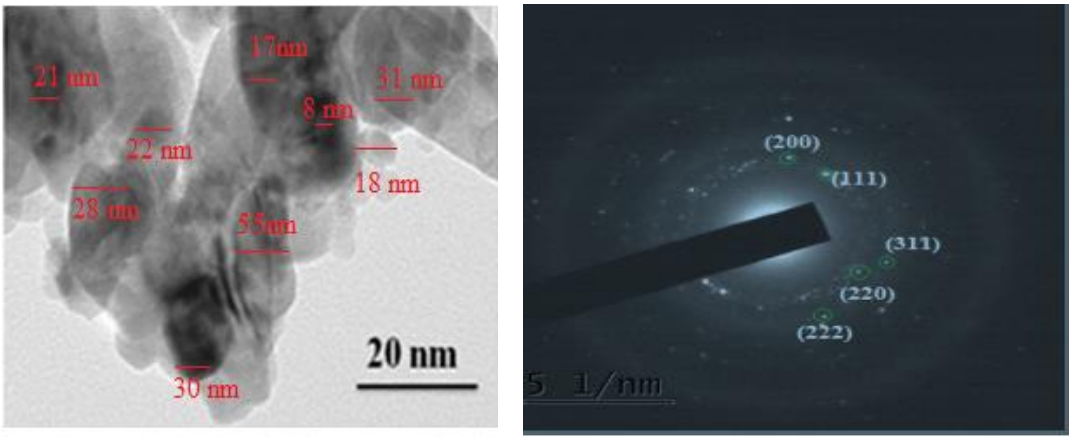

Figure 2. Photomicrographs of (a) TEM (b) SAED of pristine $CaCdAl_2O_5$ NPs.

The SEM image (Figure 3(a)) represents pristine $CaCdAl_2O_5$ NPs and PVA-NCs doped with 2, 4, 6 and 8wt% of $CaCdAl_2O_5$ NPs were displayed in Figure 3(b-e) respectively. The NPs agglomerated into a large domain showed the smooth surface of pure PVA film without any craters on the surface

of film. The varying domain sizes obtained may be due to agglomeration of the NPs, which takes place in order to minimize the high surface energy that exists in individual NPs. It can be observed that NPs were homogeneously dispersed with slightly agglomeration throughout the PVA matrix at lower dosage of fillers. At a higher dosage of fillers, the agglomeration islands of NPs in NCs have been noticed in Figure 3(e). As increase in NPs loading, the number of particles increases, so the inter particle distance decreases in PVA matrix.

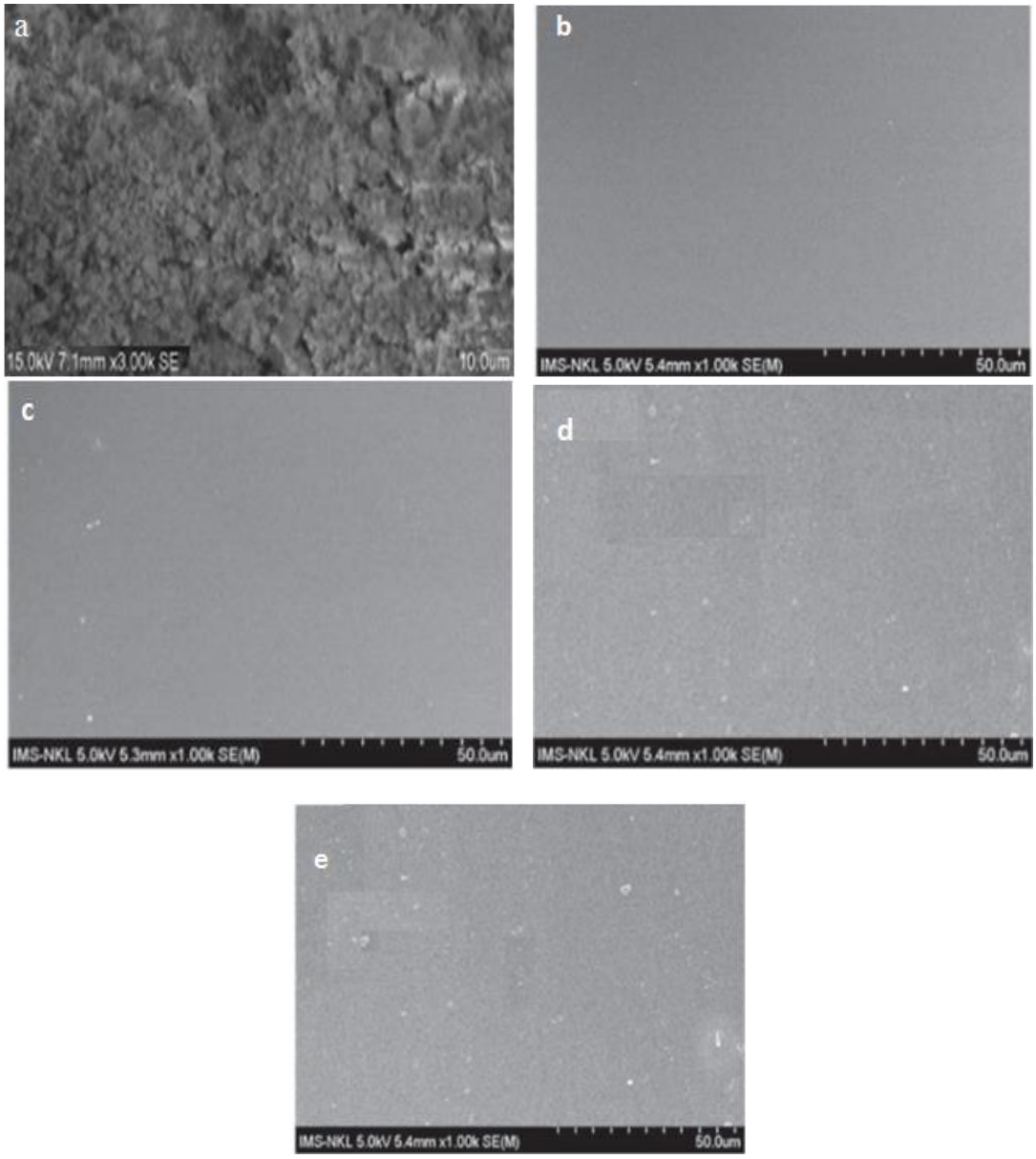

Figure 3. SEM photographs of a) $CaCdAl_2O_5$ NPs b) pure PVA c) 2 d) 4 e) 6 and f) 8wt% NPs doped PVA NCs

3.2. FTIR studies

Figure 4 (a-e) presents FTIR spectra for PVA with its NC films at wave number range 4000-500 cm^{-1}. FTIR provides information about the effects and interactions between the various constituents in the polymer NCs. The vibrational peaks at 3315, 2914, 2838,1722,1422,1248, 1085 and 836cm^{-1} are assigned to the signature vibration bands of PVA. The observed strong band at 3548–3053cm^{-1} are referred to vibrational stretching of -OH side-groups in matrix. The asymmetric vibrational stretching band corresponding to C-H occurs at 2914cm^{-1}, whilst C-H symmetric vibration stretching at 2838cm^{-1}. From Figure 4(b–e), the IR bands for $CaCdAl_2O_5$ NPs incorporated PVA NC films are show partially modified. The changes in the stretching vibration of -OH at 3548–3053$cm^{-1}$and asymmetric C-H stretching (2914cm^{-1}) affirm the changes in gross structural behaviors of PVA; refer to the effect of $CaCdAl_2O_5$ NPs in PVA matrix. The decrease in the intensities of -OH stretching vibrations and their relative broadening

may be attributed to the physical attraction between the calcium, cadmium and aluminium $CaCdAl_2O_5$ NPs with -OH groups of PVA.[28] Intensity of vibrational stretching at 1722cm^{-1} for C=O (refer to residual acetate group) showed a slightly reduced with increasing dosage of $CaCdAl_2O_5$. The peak at 1019-1087cm^{-1} of C-O group in PVA is intercalated with positive charges of $CaCdAl_2O_5$ and intensity of this peak reduces with increments NPs contents. The un-hydrolyzed acetyl groups (C-O-O) present in PVA structure exhibit vibational peak at 1250cm^{-1}. Furthermore, the peaks at 1437-1378cm^{-1} may be attributed to bending vibration of (C–H) in-plane of backbone chains. The characteristic -CH2 wagging in out-plane is found to be shifted to 880cm^{-1} and -CH2 rocking is noticed at around 658 cm^{-1}. Figure 4 (b–e) shows two IR absorption peaks at 552 and 625cm^{-1}, which clearly indicates the presence of metal oxide NPs in NC films.[29]

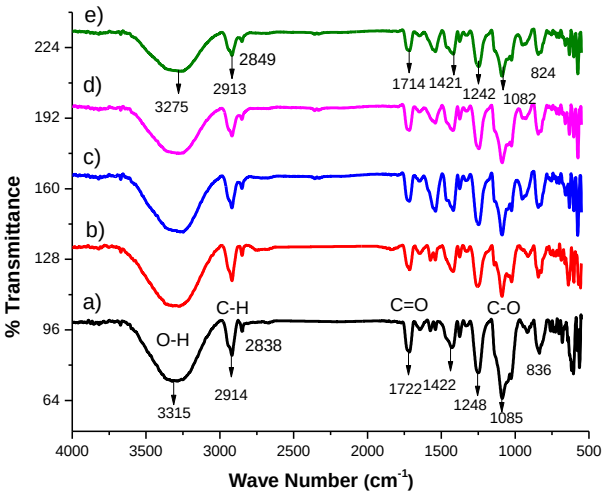

Figure 4 FTIR spectra of a) pure PVA b) 2 c) 4 d) 6 and e) 8wt% NPs doped PVA NCs

3.3. Electrical characteristics

3.3.1. Dc and Ac conduction

In NC films, the conduction is due to a mobility of charge carriers (electrons) in conduction-band and movement of holes in valence-band or hopping of carriers between localized sites in the matrix. The required energy for electronic conduction can be supplied by the applied electric field to excite a carrier and this hopping process is favored in the case of highly disordered NC films. In addition, dielectric films differ in their electrical properties according to the preparation parameters. Figure 5(a) displays current-voltage behavior of pure PVA and PVA-NCs containing 2, 4, 6, and 8wt% $CaCdAl_2O_5$ NPs. It can be discerned from Figure 5(a) that, there are two distinct regions; first region is at lower voltage, 0-5V and another region at >5V. At lower voltage region, it can be seen that the current is equal to ~ 0.1mA, which resistive is predominant manner for conduction. With a lower dosage of $CaCdAl_2O_5$ NPs in PVA matrix, the resistivity may arise caused restrict the increase of electrical current through NC film. The initial resistivity at low voltage may be attributed to impact of Coulomb barrier. Such phenomenon will occur after introduced a small dosage of NPs into polymeric matrix, where many tunneling knots may be formed and impeding the motion of charge carriers in a directional of a particular electrical field. However, the resistivity of PVA/ $CaCdAl_2O_5$ NCs decreases, with increasing the dosage of $CaCdAl_2O_5$ NPs, which move as conducting particles in PVA matrix. It can be attributed to the reduction in the distance between the NPs at higher dosage, so the utilized electrical field is sufficient to induce electrons to move from one particle into another, which leads to increase in conductivity [29-30]. At higher voltage region, the I-V curves exhibit a pronounced nonlinearity, which is clear in the NCs containing 2-8 wt % of $CaCdAl_2O_5$. The deviations in a current-voltage plots may emerge from a numeral of un-ohmic charge transmit processes like space-charge-limited current (SCLC), Schottky-conduction and Poole-Frenkel emission mechanisms.[31] In mechanism of SCLC-regime, internal carriers inside NC-film are lower than inserted carriers from electrode, which arise space-charge portions near the contacts interface and are responsible for bulk limited SCLC [32]. In Schottky-mechanism, the current attributed to the transmission of electrons between cathode (metal-electrode) and NCs. However, the conduction in Poole-Frenkel-mechanism is due to contributions of emission the

charge carriers trapped in the defect centers.[33] Thereby, to investigate the accurate emission responsible for nonlinear variation of current with voltage, a detailed analysis of the I-V behavior has been performed.

The ac-conductivity, σ_{ac} which has been obtained from LCR meter at different frequency and σ_{ac} is calculated as follow;

$$\sigma_{ac} = \frac{dG_S}{A} \quad (4)$$

where, G_s is measured conductance (S), d is sample thickness (cm) and A is sample area (cm^2). The variation of σ_{ac} for PVA NCs with 2, 4, 6 and 8 wt% of $CaCdAl_2O_5$ NPs as a function of frequency at room temperature is depicted in Figure 5(b). At lower frequency region < 7.3 KHz, Figure 5(b), showed a slightly increase in σ_{ac} where, long-range transport of charges occurs through the semiconducting islands in the insulating PVA matrix. Therefore, the rate of contribution of charge carrier is low.[34] At higher frequency region, the electron attained sufficient energy and the electrons hop from one conducting site to another through smaller inter-particle gap lead to increase in σ_{ac} of the NC.[35]. The optimum value of σ_{ac} achieved in the current study is $2.3x10^{-5}$ Scm^{-1} for PVA incorporated with 8wt% $CaCdAl_2O_5$ NPs.

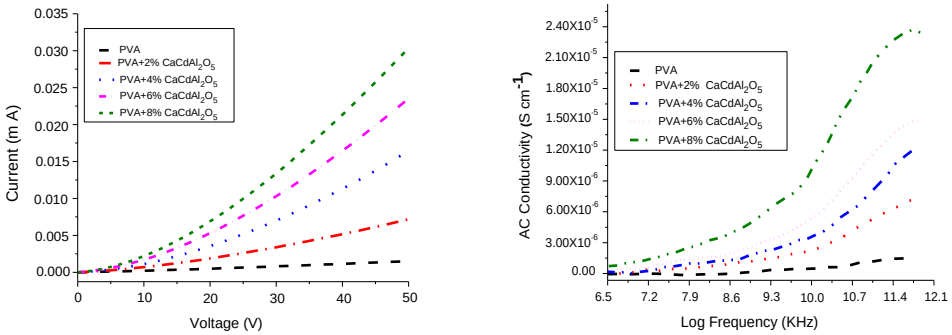

Figure. 5 (a) Dc conductivity and (b) Ac conductivity versus log frequency for PVA/$CaCdAl_2O_5$ NCs.

3.3 Optical Study

The transmittance and absorption spectra of PVA and its NC films containing 2, 4, 6 and 8 wt% of $CaCdAl_2O_5$ NPs are shown in Fig. 6(a, b). The absorption spectra of PVA in the range 220 to 250 nm is due to the π→ π* electronic transition (k-band) from the unsaturated C=O of residual acetate group present in a PVA structure and C=C which may survive in the tail head of the polymer. The absorption peak is the range of 250-300 nm, and maximum absorption peak is about 219 nm is shown in Fig. 6a, which is due to electronic transition (n→ π*) of hydroxyl group in PVA chains, further the PVA has shown no absorption in visible region (above 400nm) because it is highly transparent film. The absorption peak in the UV range increases with increase in the content of NPs in the NCs films.

The transmittance spectra of the nanocomposite films are shown in the Fig. 6(b). The pure thin film shows the high transmittance of about 89.6% and 2, 4, 6 and 8wt% NPs doped PVA thin film reduces the transmission into 45.2, 30.65, 22.40 and 9.36% respectively. Hence the transparency of the nanofilms reduced with the increase in the content of NPs in NCs films.

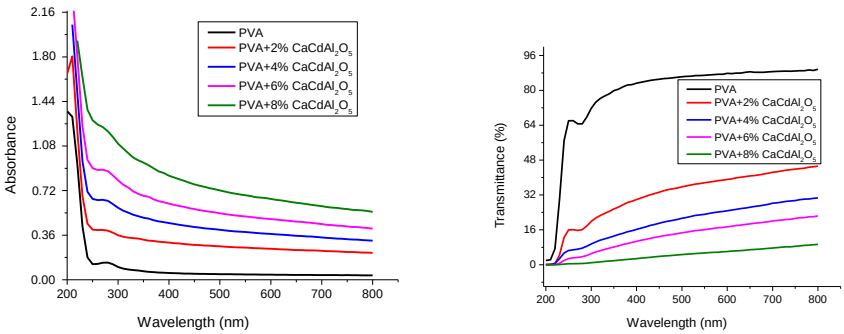

Fig .6 (a) UV Absorption (**b)** transmittance spectra for PVA/$CaCdAl_2O_5$ NCs

The direct and indirect band gap energy of PVA/ $CaCdAl_2O_5$ NCs were plotted using Tauc's plot method. In the Fig. 7a the value of the optical energy gap for an PVA material which is an insulator is around 5.34 eV for 2, 4, 6 and 8 wt% are 4.02 eV, 3.97 eV and 3.78 eV respectively. The band gap energies from 5.34 eV to 3.78 eV is been decreased with an increase in doping level from 0 to 8wt%. The increase in the concentration of NPs in PVA increases the number of molecular dipoles. These dipoles create localized sites between the valence and conducting energy bands, making lower energy transition feasible. The observed changes in the energy gap with increasing the nanoparticles wt% dopant may be due to the development of charge move complexes between $CaCdAl_2O_5$ nanoparticles and -OH groups of PVA polymer. The band gap materials are suitable for opto-electronic applications. The band gap energy is calculated by the equ. (6) [36]

$$ah\upsilon = C(h\upsilon - E_g)^{r} \quad (5)$$

where, C is a constant, E_g is optical energy band gap of the material and the exponent r is an index that depends on the nature of electronic transition, where r = ½ for direct allowed transitions, r = 2 for indirect allowed transitions.

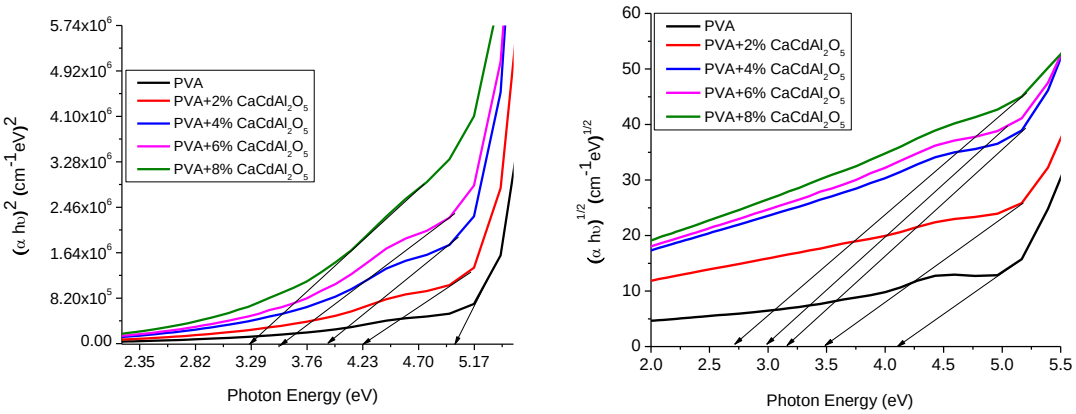

Fig. 8 Tauc's plots of **a)** direct and **b)** indirect band gap transitions as a function of photon energy for PVA/ $CaCdAl_2O_5$ NCs

The absorption co-efficient (α) as a function of the photon energy ($h\upsilon$) for pure and doped PVA films is as shown in the Fig. 9a and it can be calculated by using the equ. (7) [37]

$$\alpha = \left(\frac{2.303A}{l}\right) \quad (6)$$

where, A is the absorption and l is the thickness of the film.

From Fig. 9(a, b) The optical parameters such as refractive index (n) and Absorption coefficient (α) are essential to select the materials for a specific optoelectronic application. Figure 9(b) illustrates the n of PVA/$CaCdAl_2O_5$ NCs as a function of wavelength. From the reflectance (R) and the optical extinction data, the n can be estimated using eq. (1) as follows: We can observe that the refractive index (n) is gradually increased and then decreased significantly in the UV region with respect to the incident light wavelength and then it become constant at visible region above 400 nm for all nanocomposite thin film. The refractive index (n) obtained values for pure PVA and PVA incorporated with 2, 4, 6 and 8wt% PVA/ $CaCdAl_2O_5$ NCs. The refractive index (n) is maximum for 8 wt% NCs and it is 2.14 and 1.17 for pure PVA. The increase of refractive index for higher doping concentration is for the number of atomic refraction due to the increase of the linear polarization which has a strong bond between the particles through electrostatic interaction. The refractive index is calculated using the equ. (7)

$$n = \sqrt{\frac{4R}{1-R2} - K} + \frac{1-R}{1+R} \quad (8)$$

where, K is the extinction coefficient (K = αλ/4π)

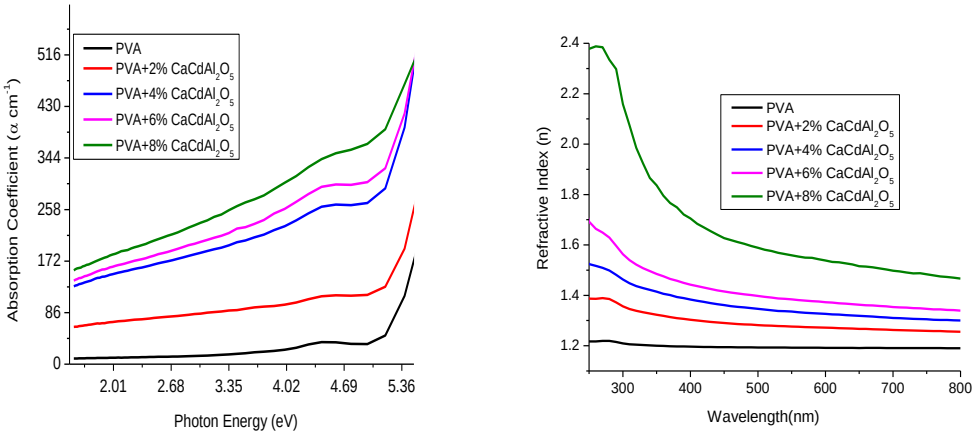

Figure. 9 a) Absorption coefficient **b**) Refractive index for PVA/$CaCdAl_2O_5$ NCs

Optical conductivity (σ) and Extinction co-efficient (*k*)

The optical conductivity (σ) is one of the main property, it gives the optical response of the material to the diffusion of charge carriers electrons due to the incident photon energy excitation, the optical conductivity depends on the refractive index (n) and absorption coefficient (α). The optical conductivity (σ) of PVA and PVA/ $CaCdAl_2O_5$ NCs is shown in Fig. 10a.

Where c is the speed of light, α is the absorption coefficient and n is the refractive index. The variation of optical conductivity as a function of wavelength is shown in the Fig. 10a. It is clearly observed that, optical conductivity; increases with increase in concentration of NPs. Further, increase in concentration of NPs results in decrease of the optical conductivity. The maximum conductivity of is achieved for 4% doped NCs film is 2.623E10 S^{-1} at 246 nm .The optical conductivity was found to be gradually increases after 260 nm, correlated with gradual increase in absorption coefficient for all samples. This is due to the charge carrier is increased and formation of a localized tail state in band gap causes the transition electrons from valence band to the nearest level state easily and band gap will be minimized. Also decrease the polymer film degree of crystallinity will decrease the band gap and increase the optical conductivity. The optical conductivity was obtained by using the equ. (9).

$$\sigma = \alpha nc/4\pi \quad (9)$$

The extinction coefficient parameters shows the energy loss due to absorbing or scattering occurs by the particles and molecules found in the substance. It can be seen from the Fig. 10(b) that *k* increases with the increase of the doping concentration this is related to the increase of the absorption coefficient. The extinction coefficient of the sample is increased with increase in doping concentration, this is because of the incident photon has adequate energy that causes an excitation of the electron from its initial state to another state [38, 39]. The extinction co-efficient is calculated using the equ. (10)

$$(K = \frac{\alpha\lambda}{4\pi}) \quad (10)$$

where, α is the absorption coefficient**.**

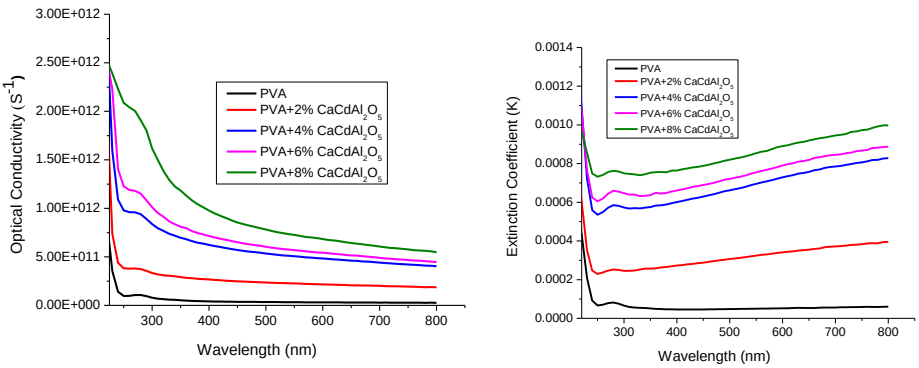

Figure. 10 a. Optical Conductivity **b.** Extinction co-efficient for PVA/ $CaCdAl_2O_5$ NCs

Optical Dielectric properties

Dielectric constant is an important characteristic of optical material. It has both real and imaginary parts [26]. Dielectric constant tells us about permittivity and polarizability of substances is related with density of states in the forbidden energy gap. The real part Fig. 11a of the dielectric constant provides information about the speed of light, which can be reduced by the materials. The imaginary part shown in Fig. 11b represents the energy absorbed by the electric field due to dipole motion [40]. The real part mainly depend on (n2) value and imaginary part mainly depend on (k) values, increase the dielectric constant with increasing the photon energy is due to the interference between the photon and electron of the PVA polymer thin film. The real part of the dielectric constant give us the material ability to slow down the light speed through it and the imaginary part of dielectric constant give us the dielectric material energy to form an electric field due to dipole movement. The real and imaginary dielectric constant was calculated using an equ. (11) and (12)

$$(\varepsilon_r = n^2 - k^2) \quad (11)$$

$$(\varepsilon_i = 2nk) \quad (12)$$

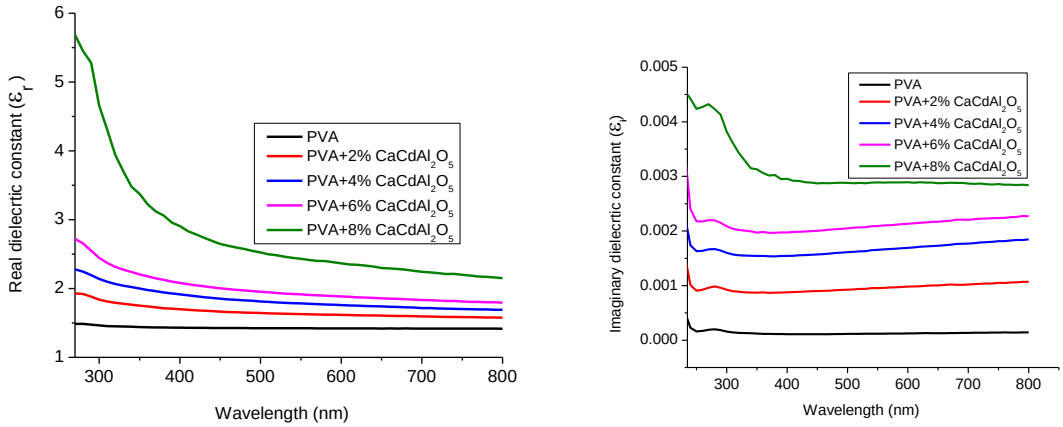

Figure. 10 a. real **b.** imaginary dielectric constant for PVA/ $CaCdAl_2O_5$ NCs

3.4 Thermal studies

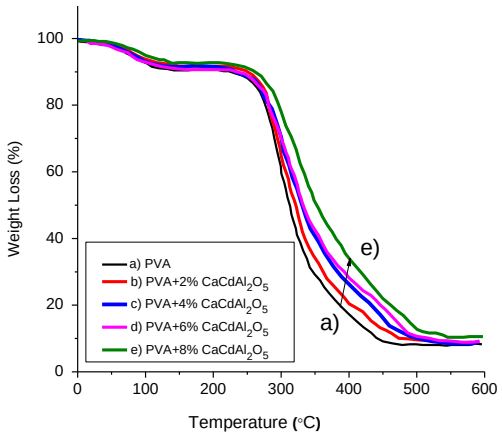

Figure. 11 TGA thermogram graphs of pristine PVA and its PVA/ $CaCdAl_2O_5$ NCs

The thermal studies of pure PVA and PVA composites films were carried out to assess their thermal stability. The TGA thermograms of Pristine PVA, 2, 4, 6 and 8 wt% of nano $CaCdAl_2O_5$ NPs incorporated PVA composites (Fig. 11a–d) showed three steps degradation processes. It is keenly observed that the initial degradation temperature was found to be increased gradually with an increasing $CaCdAl_2O_5$ filler concentration onto PVA matrix. The first step degradation process started around 205°C for pure PVA, 210°C (2 wt%.NC), 220°C (4 wt%.NC) 228°C (6 wt%.NC) and 236°C for 8wt%. PVA composite films. This decomposition process was intended due to the removal of moisture, physisorbed and chemisorbed water molecules [41]. On further raise in temperature will induce the major decomposition of polymer

chain. The second major weight loss was started around 277, 286, 294, 300 and 305°C for pure PVA to 8wt% NCs which was running approximately up to 435°C for pure PVA and all the three composite films. This was happened due to the breaking of intermolecular hydrogen bonding which led to the degradation of PVA backbone. The third major weight loss started above 440°C with the slight shift to higher value for all the nano composite doped PVA composite films when compared with the pure PVA. The intercalated polymer chains were started decomposing by leaving a plateau region [42] with constant mass beyond 500°C. A constant mass of about 10-18% was obtained after 500°C for all the composite films which may be due to the formation of carbonaceous mass in the form of layer on the polymer surface during the degradation of polymer chains that normally restrict further decomposition of polymer. The PVA/ $CaCdAl_2O_5$ composites with enhanced thermal stability have been reported in the literature [43]. This may be due to the interaction of nano CdO with hydroxyl groups of PVA. It is the tendency of Cd^{2+} Ca^{2+} and Al^{3+} ions of $CaCdAl_2O_5$ used to form a complex with the OH groups of PVA. Moreover, $CaCdAl_2O_5$ particles exhibit a notable surface catalytic and complex formation effect which remarkably strengthens the PVA backbone thereby creating C=C in the polymer chain. As the combined effect of surface catalytic and chelating nature, the thermal stability of PVA/ $CaCdAl_2O_5$ composites is improved slightly when compared with pure PVA

3.5 Cyclic voltmmetry studies

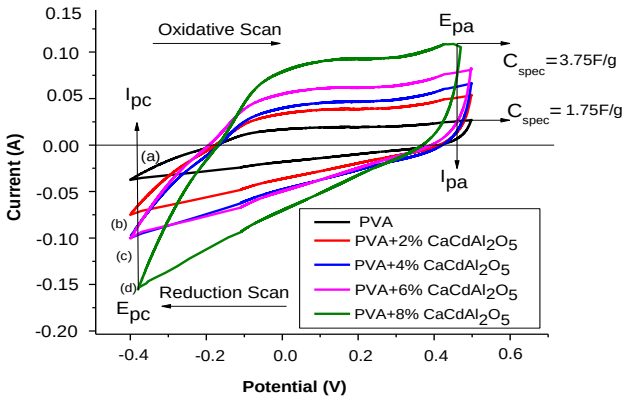

Figure. 12. The cyclo voltammetry graphs of pristine PVA and its PVA/ $CaCdAl_2O_5$ NCs

The CV was recorded at room temperature by employing three electrode cells with platinum wire as an auxiliary electrode, Ag/AgCl electrode as the reference electrode and NC films as the working electrode. The 2 M KOH is used as a electrolyte solution. The scanning was carried out in the voltage range from 0 to 1 V at scan rate of 10 mVs^{-1}[44]. The CV performed for PVA/$CaCdAl_2O_5$ NCs is presented in Fig. 12. From Fig. 13, the CV for pure PVA has the common reversible electrochemical behaviour which occurs due to oxidation of hydroxyl group and reduction of carbonyl groups in the PVA polymer structure. The onset of the oxidation potential for *E*onset(oxd) for PVA is around -0.393 V, while the PVA-doped 8 wt% $CaCdAl_2O_5$ NC shows a decrement in *E*onset(oxd) values to -0.389 V. This is because the $CaCdAl_2O_5$ NPs make a continuous conduction path in the PVA and form a charge transfer complex (CTC) which makes the movement of charge carriers between thin film and the electrolyte. A steady potential (V) region obtained over -1 to 5 V where the PVA/ $CaCdAl_2O_5$ heterogeneous mixture NCs has a higher dielectric constant directing to stability of electro-chemical window and film does not undergo any chemical deformation within potential region [45, 46]. The current density of the CV curve of the NC films is wide and the duck shape which indicates the increment in the specific capacitance, C_{spec}, values with increasing $CaCdAl_2O_5$ NPs from 2 to 8 wt% in PVA-NC films. The specific capacitance C_{spec} of PVA-NCs is calculated as follows [47]:

$$C_{spec} = \frac{\int_{v1}^{v2} I.dv}{Vm\,\Delta v} \quad (13)$$

where V is the scan rate (Vs^{-1}) I is the response current (A) (response of the average integral area of CV curve), m is the mass of material, Δv is the difference between the lowest and highest potential (*V*). The calculated C_{spec} values show a significant enhancement in C_{spec} from 1.75F/g for

pure PVA to 3.75F/g for PVA/ 8wt% $CaCdAl_2O_5$ NC

Conclusion

The PVA/ $CaCdAl_2O_5$ nanocomposite with different concentration of nanoparticles were prepared by solution intercalation technique. The XRD analysis result shows that the crystal structure of nanoparticles, these NPs had a negative effect on crystallinity nature of PVA which indicates that increase the amorphous portion of nanocomposites. The broadening and shift of peak in XRD of nanocomposites film is due to the growth of micro strain & different Crystallite size due to structure deformation, where FTIR shows a force of attraction occurs between the elements. The SEM Image reveals that nanoparticle has average diameter of 30 nm. By increasing the $CaCdAl_2O_5$ dopant into PVA the UV absorption of film were enhanced and the direct energy band gap decreases from 5.34 eV to 3.28 eV, it obeys direct electron transition. The increase of extinction co-efficient (*k*) related to that photon with small energy scattered and their energy losses, refractive index (*n*) Increased with the wt% of $CaCdAl_2O_5$ nanoparticles due to high change density. The calculated C_{spec} values show a significant enhancement in C_{spec} from 1.75F/g for pure PVA to 3.75F/g for PVA/ 8wt% $CaCdAl_2O_5$ NCs.This result reveals that these nanocomposites are promising materials for optoelectronics and energy storage application.

References

1. Gleiter H (2000) Nanostructured materials: basic concepts and microstructure. Acta materialia 1;48(1):1-29.
2. Gayitri, H.M., Al-Gunaid, M.Q., AL-Ostoot, F.H., Al-Zaqri, N., Boshaala, A. and Gnanaprakash, A.P., 2023. Investigation on opto-electrical, structural and electro-chemical performance of PVA/$ZnBi_2MoO_7$ hybrid nanocomposites. Polymer Bulletin, 80(1),773-790.
3. Zhou L, Jiang Y (2020) Recent progress in dielectric nanocomposites. Materials Science and Technology. 2;36(1):1-6.
4. Heiba ZK, Mohamed MB (2019) Effect of annealed and Mg-doped nano ZnO on physical properties of PVA. Journal of Molecular Structure. 1181:507-17.
5. El-Shamy AG, Zayied HS (2020) New polyvinyl alcohol/carbon quantum dots (PVA/CQDs) nanocomposite films: structural, optical and catalysis properties. Synthetic Metals. 259:116218.
6. Gayitri HM, Al-Gunaid M, Prakash AP (2020) Optical, structural and thermal properties of hybrid PVA/CaAl2ZrO6 nanocomposite films.
7. Dang ZM, Yuan JK, Zha JW, Zhou T, Li ST, Hu GH (2012) Fundamentals, processes and applications of high-permittivity polymer–matrix composites. Progress in materials science. 57(4):660-723.
8. Heiba ZK, Mohamed MB, Ahmed SI, Albassam AA (2020) Structural, optical, and electronic properties of non-stoichiometric nano-ZnS 1− x: Mn x. Journal of Materials Science: Materials in Electronics. 31(16):13447-59.
9. Chebil A, Doudou BB, Dridi C, Dammak M (2019) Synthesis characterization, optical and electrical properties of polyvinyl alcohol/multi-walled carbon nanotube nanocomposites: a composition dependence study. Materials Science and Engineering: B. 243:125-30.
10. Sheha E, Khoder H, Shanap TS, El-Shaarawy MG, El Mansy MK (2012) Structure, dielectric and optical properties of p-type (PVA/CuI) nanocomposite polymer electrolyte for photovoltaic cells. Optik. 123(13):1161-6.
11. Alhazime AA, Mohamed MB, Abdel-Kader MH (2019) Effect of Zn 1- x Mg x S doping on structural, thermal and optical properties of PVA. Journal of Inorganic and Organometallic Polymers and Materials. 29(2):436-43.
12. Bacaksiz EM, Parlak ME, Tomakin MU, Özçelik A, Karakız M, Altunbaş M (2008) The effects of zinc nitrate, zinc acetate and zinc chloride precursors on investigation of structural and optical properties of ZnO thin films. Journal of Alloys and Compounds. 466(1-2):447-450.
13. Mohammad MT, Hashim AA, Al-Maamory MH (2006) Highly conductive and transparent ZnO thin films prepared by spray pyrolysis technique. Materials Chemistry and Physics. 99(2-3):382-387.
14. Yi GC, Wang C, Park WI (2005) ZnO nanorods: synthesis, characterization and applications. Semiconductor science and technology. 20(4):S22.
15. Salman TA, Raheem HM (2020) Electrophoresis Deposition of Tungsten oxide Nanoparticles for Corrosion Inhibition. InJournal of Physics: Conference Series (Vol. 1664, No. 1, p. 012053). IOP Publishing.

16. El-Mansy MK, Sheha EM, Patel KR, Sharma GD (2013) Characterization of PVA/CuI polymer composites as electron donor for photovoltaic application. Optik. 124(13):1624-31.
17. Al-Gunaid, M.Q., Shashikala, B.S., Gayitri, H.M., Alkanad, K., Al-Zaqri, N., Boshaala, A. and Al-Ostoot, F.H., 2022. Characterization of Opto-Electrical, Electrochemical and Mechanical Behaviors of Flexible PVA/(PANI+ La_2CuO_4)/$LiClO_4$-PC Polymer Blend Electrolyte Films. Macromolecular Research, 30(9), pp.650-658.
18. Talam S, Karumuri SR, Gunnam N (2012) Synthesis, characterization, and spectroscopic properties of ZnO nanoparticles. International Scholarly Research Notices.
19. Sadikov, G.G., Shishakov, N.A., Izv. Akad (1965) Nauk SSSR, Ser. Khim., 1277
20. Donnay, Nowacki., Crystal Data, Anal (1938), Chem., 10, 475.
21. Kaler V, Pandel U, Duchaniya RK (2018) Development of TiO_2/PVA nanocomposites for application in solar cells. Materials Today: Proceedings. 5(2):6279-87.
22. Ali FM, Kershi RM, Sayed MA, AbouDeif YM (2018) Evaluation of structural and optical properties of Ce3+ ions doped (PVA/PVP) composite films for new organic semiconductors. Physica B: Condensed Matter. 538:160-6
23. Sengwa RJ, Choudhary S (2014) Structural characterization of hydrophilic polymer blends/montmorillonite clay nanocomposites. Journal of Applied Polymer Science. 131(16).
24. Godavarti U, Mote VD, Dasari M (2017) Role of cobalt doping on the electrical conductivity of ZnO nanoparticles. Journal of Asian Ceramic Societies. 5(4):391-6.
25. Borah MN, Baruah BJ, Chaliha S, Gogoi DP, McFarlane U, Dutta S (2013) Structural analysis of chemically deposited nanocrystalline CdSe films. Journal of Experimental Nanoscience. 8(3):273-9.
26. Rahimi-Nasrabadi M, Pourmortazavi SM, Rezvani Z, Adib K, Ganjali MR (2015) Facile synthesis optimization and structure characterization of zinc tungstate nanoparticles. Materials and Manufacturing Processes. 30(1):34-40.
27. Chithambararaj A, Sanjini NS, Velmathi S, Bose AC (2013) Preparation of h-MoO_3 and α-MoO 3 nanocrystals: comparative study on photocatalytic degradation of methylene blue under visible light irradiation. Physical Chemistry Chemical Physics. 15(35):14761-9.
28. Rahimi-Nasrabadi M, Pourmortazavi SM, Ganjali MR, Hajimirsadeghi SS, Zahedi MM (2013) Electrosynthesis and characterization of zinc tungstate nanoparticles. Journal of Molecular Structure. 1047:31-6.
29. Aprilliza M (2017) Characterization and properties of sodium alginate from brown algae used as an ecofriendly superabsorbent. InIOP conference series: materials science and engineering (Vol. 188, No. 1, p. 012019). IOP Publishing.
30. Sen SK, Paul TC, Manir MS, Dutta S, Hossain MN, Podder J (2019) Effect of Fe-doping and post annealing temperature on the structural and optical properties of MoO_3 nanosheets. Journal of Materials Science: Materials in Electronics. 30(15):14355-67.
31. Gayitri HM, AL-Gunaid M, Gnana Prakash AP (2020) Investigation of triplex $CaAl_2ZnO5$ nanocrystals on electrical permittivity, optical and structural characteristics of PVA nanocomposite films. Polymer Bulletin. 2020 Sep;77(9):5005-26.
32. Umapathy V, Neeraja P, Manikandan A, Ramu P (2017) Synthesis of NiMoO4 nanoparticles by sol–gel method and their structural, morphological, optical, magnetic and photocatlytic properties. Transactions of Nonferrous Metals Society of China. 27(8):1785-93.
33. Sudhamani SR, Prasad MS, Sankar KU (2003) DSC and FTIR studies on gellan and polyvinyl alcohol (PVA) blend films. Food Hydrocolloids. 17(3):245-50.
34. Gayitri HM, AL-Gunaid M, Gnana Prakash AP (2020) Investigation of triplex $CaAl_2ZnO_5$ nanocrystals on electrical permittivity, optical and structural characteristics of PVA nanocomposite films. Polymer Bulletin. 77(9):5005-26.
35. Al-Gunaid MQ, Saeed AM, HM G, Basavarajaiah S (2020) Impact of nano-perovskite La_2CuO_4 on dc-conduction, opto-electrical sensing and thermal behavior of PVA nanocomposite films. Polymer-Plastics Technology and Materials. 59(5):469-83.
36. El Sayed AM, El-Sayed S, Morsi WM, Mahrous S, Hassen A (2014) Synthesis, characterization, optical, and dielectric properties of polyvinyl chloride/cadmium oxide nanocomposite films. Polymer composites. 35(9):1842-51.
37. Mahmoud WE, Al-Ghamdi AA, Al-Agel F (2011) Synthesis and optical properties of

poly (vinyl acetate)/bismuth oxide nanorods. Polymers for Advanced Technologies. 22(12):2055-61.

38. Gayitri HM, Al-Gunaid M, Prakash AP (2020) Optical, structural and thermal properties of hybrid PVA/$CaAl_2ZrO_6$ nanocomposite films. nopr.niscair.res.in
39. Liu JG, Ueda M (2009) High refractive index polymers: fundamental research and practical applications. Journal of Materials Chemistry. 19(47):8907-19.
40. Basha MA (2010) Magnetic and optical studies on polyvinylpyrrolidone thin films doped with rare earth metal salts. Polymer journal. 42(9):728-34.
41. H. M. Gayitri , Al-Gunaid M, BS M, Siddaramaiah B, A. P GP (2019) Structural, dielectric permittivity and optical characteristics of casting poly vinyl alcohol/calcium nickel aluminate nanocomposite films. Polymer-Plastics Technology and Materials. 58(10):1110-24.
42. Gayitri, H.M., Al-Gunaid, M.Q. and Kumar, J.R., 2022. Investigation on optical, structural and electrochemical properties of hybrid PVA/$ZnWMoO_7$ nanocomposite film for optoelectronics and super capacitor applications. Polymer Bulletin, 1-19.
43. El Sayed AM, Morsi WM (2014) α-Fe 2 O 3/(PVA+ PEG) nanocomposite films; synthesis, optical, and dielectric characterizations. Journal of Materials Science. 49(15):5378-87.
44. Al-Gunaid MQ, Saeed AM (2018) Effects of the electrolyte content on the electrical permittivity, thermal stability, and optical dispersion of poly (vinyl alcohol)–cesium copper oxide–lithium perchlorate nanocomposite solid polymer electrolytes. Journal of Applied Polymer Science. 135(8):45852.
45. Choudhary S (2018) Structural, optical, dielectric and electrical properties of (PEO–PVP)–ZnO nanocomposites. Journal of Physics and Chemistry of Solids. 121:196-209.
46. Soliman TS, Vshivkov SA (2019) Effect of Fe nanoparticles on the structure and optical properties of polyvinyl alcohol nanocomposite films. Journal of Non-Crystalline Solids. 519:119452.
47. Choudhary S (2018) Characterization of amorphous silica nanofiller effect on the structural, morphological, optical, thermal, dielectric and electrical properties of PVA–PVP blend based polymer nanocomposites for their flexible nanodielectric applications. Journal of Materials Science: Materials in Electronics. 29(12):10517-34.